electronics

MDPI

Article

A Bidirectional Simultaneous Wireless Power and Data Transfer System with Non-Contact Slip Ring

Yuanshuang Fan [1], Qiurui Chen [1,*], Sihan Wu [1], Jing Xiao [2] and Zhihui Wang [1]

[1] College of Automation, Chongqing University, Chongqing 400044, China; fanyuanshuang@cqu.edu.cn (Y.F.); 202013131136@stu.cqu.edu.cn (S.W.); wangzhihui@cqu.edu.cn (Z.W.)
[2] Southern Power Grid Corporation Wireless Power Transmission Joint Laboratory, Guangxi Power Grid Company Ltd., Nanning 530023, China; xiao_j.sy@gx.csg.cn
* Correspondence: chenqiurui@cqu.edu.cn

Abstract: A non-contact slip ring is proposed in this paper. The bidirectional simultaneous wireless power and data transfer (BD-SWPDT) technology is utilized to transfer power and data bidirectionally. A bidirectional constant-voltage LC hybrid compensation topology is proposed, which utilizes the LC series parallel structure to have different equivalent models at different frequencies. By using different operating frequencies for forward and reverse power transfer, the system's forward and reverse transfer can be equivalent to different constant-voltage output compensation topologies. The resonant parameters of the system are designed to achieve consistent voltage gain for forward and reverse power transfer. And based on this topology, a data carrier injection method is designed to achieve high Signal Noise Ratio (SNR) simultaneous data transfer. To improve the flexibility of non-contact slip ring installation, a caliper-type coupling structure is proposed. Finally, the feasibility of the proposed method is verified through experiments, achieving a forward and reverse output power of 200 W and half duplex communication with a data rate of 19.2 kbps.

Keywords: wireless power transfer; contactless slip ring; simultaneous wireless power and data transfer (SWPDT); caliper type coupling structure

Citation: Fan, Y.; Chen, Q.; Wu, S.; Xiao, J.; Wang, Z. A Bidirectional Simultaneous Wireless Power and Data Transfer System with Non-Contact Slip Ring. *Electronics* **2024**, *13*, 3974. https://doi.org/10.3390/electronics13203974

Received: 2 September 2024
Revised: 29 September 2024
Accepted: 4 October 2024
Published: 10 October 2024

1. Introduction

Magnetic Coupled Wireless Power Transfer (MC-WPT) technology is based on the principle of electromagnetic induction, which achieves the transmission of electrical power through non-contact means, directly avoiding physical contact between rotating structures and providing an effective means for the development of electrical power transmission technology for rotating structures [1,2]. With the development of WPT technology, it has been applied in multiple fields, such as smart homes, mobile phones, electric vehicles, and medical devices [3–8]. In addition, it has gradually been applied in some special industries, such as wireless power supply in underwater environments [9,10] and rotary guidance systems in the field of oil drilling [11].

In recent years, rotating equipment has gradually been applied in various fields of our lives, especially in some very important areas, such as satellites, helicopters, radars, oil drilling, and wind power generation [12]. During the operation of the equipment, it is necessary to transmit the electrical power from the stator side to the rotor side, and at the same time, the sensor signals on the rotor side also need to be transmitted back to the host for internal operation and control. Due to the need for the device to rotate 360°, in order to prevent cable entanglement, the internal power transmission of the rotating structure is usually achieved through conductive slip rings. For the wireless power transfer of rotary structures, wireless power transfer technology with rotary structures has been widely studied. A wireless power transfer rotary structure for a solar wing is proposed in [12], a multi-U-shaped column rotary transformer is proposed in [13], and a mixed flux coupler is proposed in [14]. The couplers adopted in these papers are traditional coaxial nested slip

rings. However, the flexibility of this type of coupler is not high, and only unidirectional power transfer is achieved without simultaneous data transfer. End-to-end couplers are also proposed in [15–18] and Series or None compensation is adopted in these papers, which will cause serious interference to data transfer when data are simultaneously transferred sharing the same coupler [19]. In practical applications, in addition to power transfer, simultaneous wireless data transfer is also needed. A simultaneous wireless power and data transfer method adopting a half-cylinder stator and quarter-cylinder rotator coupler is proposed in [20], which achieves simultaneous data transfer while supplying power to rotating equipment. However, extra coils for data transfer are added in the coupler, which will reduce the flexibility of the coupler. In some rotating applications, such as a satellite solar wing, batteries are usually stored inside the satellite; when there is sunlight, solar panels absorb solar radiation and convert it into electrical energy to power devices such as sail sensors. At the same time, the electrical energy is transmitted to the satellite's internal battery for storage through conductive slip rings. While the satellite operates in the shadow of the sun, the electrical energy in the battery is released to provide power for the equipment. The sensor devices on the solar panel need to be powered through conductive slip rings. In the process of power transfer, it is also necessary to transmit control data to control the operation of sensors and other equipment on solar panels, and to transmit sensor data through slip rings to the satellite for processing. These demands can be exactly met by a BD-SWPDT system.

A bidirectional simultaneous wireless power and data transfer (BD-SWPDT) system with non-contact slip ring based on caliper type coupling structure is proposed in this paper. A bidirectional constant-voltage LC hybrid compensation topology and a BD-SWPDT topology are proposed, and a caliper-type coupler is designed to improve system flexibility. In the power transfer channel, based on the capacitive or inductive characteristics of LC series and parallel networks at different frequencies, by controlling the frequency during bidirectional power transfer, the system topology is equivalent to different constant-voltage output topologies in forward and reverse power transfer, achieving constant voltage output during bidirectional power transfer. For data transfer, amplitude shift keying (ASK) is adopted, the coupler is frequency division multiplexed, and parallel networks with a center frequency of the data carrier to achieve the impedance isolation of the power and data transfer channel are added. Finally, bidirectional simultaneous wireless power and data transfer is achieved through the same caliper-type coupling structure. The proposed system has the following features:

(1) Simultaneous wireless power and data transfer through a pair of coupled coils;
(2) An on-contact slip ring based on a caliper-type coupling structure is utilized to replace the traditional contact slip ring equivalently;
(3) Bidirectional power transfer with independent transfer gains is achieved;
(4) A constant-voltage output topology with band-pass filtering characteristics is proposed, achieving constant voltage output and suppressing the power interference on simultaneous data transfer.

This paper is organized as follows. In Section 2, a structural diagram of the BD-SWPDT system is shown. In Section 3, the bidirectional power transfer channel is analyzed based on its circuit models, and its operation principle is illustrated. In addition, the caliper-type coupler is analyzed through simulation. In Section 4, the structure of the simultaneous data transfer channel is proposed, and its operation principle is illustrated. In Section 5, an experimental prototype is built to verify the correctness of the theoretical analysis and the feasibility of the proposed system. In Section 6, a discussion is offered, and the results of the proposed system are compared with the references. Finally, a conclusion is drawn in Section 7.

2. System Overview

The structural diagram of the proposed BD-SWPDT is shown in Figure 1. The power transfer channel and the data transfer channel share the same pair of coupled coils. In the

power transfer channel, when electrical power flows in the forward direction, a driving signal is applied on the primary active bridge and the active bridge operates in an inverter mode to generate high-frequency voltage. The reactive power of the system is compensated by a compensation network, and an alternating magnetic field is generated on the primary coil. The reactive power of the system is also compensated by a compensation network on the secondary side. The secondary active bridge is not applied on a driving signal, or operates in a rectification mode using a control strategy to convert AC into DC, thereby achieving the forward transmission of electrical power. Similarly, when electrical energy flows in the opposite direction, a secondary side active bridge is applied on a driving signal and operates in inverter mode, while the primary side is in rectification mode. The system achieves bidirectional power transfer by controlling the driving signals of the primary and secondary sides. In the data transfer channel, when data are forward-transferred, the data are modulated onto a high-frequency carrier through a modulation module, and the high-frequency carrier is injected into the primary coils through the data carrier injection module. On the secondary side, the carrier is extracted by the data carrier extraction module and demodulated by the data demodulation module to recover the data. Due to the symmetric structure of the data transfer channel, the process of reverse data transfer is the same as forward data transfer.

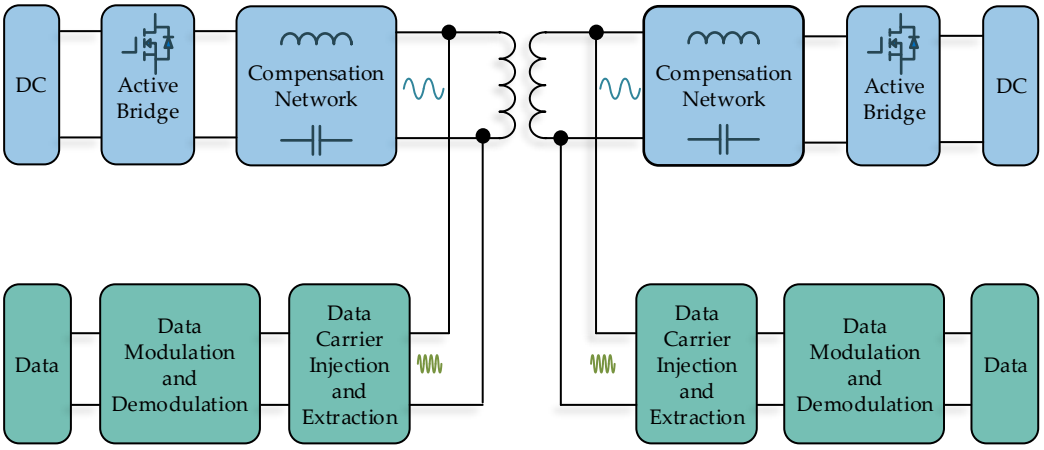

Figure 1. The BD-SWPDT system's structural diagram.

3. Bidirectional Power Transfer Channel

3.1. The Topology of the Power Transfer Channel

When power and data are transferred simultaneously via the same pair of coupled coils, the data transfer channel will be greatly interfered with by the harmonics components of the power transfer channel. To suppress the interference of the power transfer channel, compensation topologies with band-pass filtering characteristics such as LCC compensation topology are usually adopted in both sides of an SWPDT system [19]. A bidirectional constant voltage LC hybrid compensation topology is proposed in the paper, as shown in Figure 2. Based on the capacitive or inductive characteristics of LC series in parallel networks at different frequencies, the system topology is equivalent to different constant-voltage output topologies in the forward and reverse transmission processes, controlling the frequency during the bidirectional transmission of electrical power, and achieving constant-voltage output in the bidirectional transmission process. U_{dc1} and U_{dc2} are equivalent DC power sources for forward and reverse power transfer. L_p and L_s are the self-inductance of the primary and secondary coils, M is the mutual inductance of the coupled coils, I_p and I_s are the current of the primary and secondary side coils, U_{Lp} and U_{Ls} are the voltages of the primary and secondary side coils, U_p and I_1 are the voltage and current of the primary side inverter, U_s and I_2 are the voltage and current of the secondary side inverter, and C_{d1} and C_{d2} are the input or output filtering capacitors. S_1–S_4 and S_5–S_8 represent the active bridges composed of four MOSFETs on the primary and secondary sides, respectively, and they

are used to achieve DC inversion and controllable rectification in the bidirectional power transfer. LC hybrid compensation topologies are adopted on the primary and secondary sides of the system.

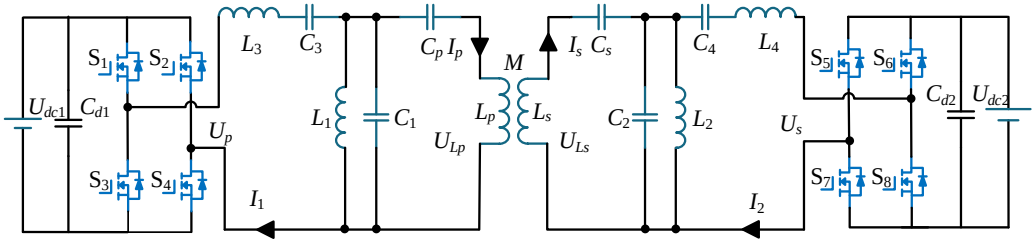

Figure 2. The topology of the BD-WPT system.

The forward and reverse power transfer adopts different operating frequencies. In this paper, the operating frequency of the forward power transfer is f_f, the operating frequency of the reverse power transfer is f_r, and $f_f < f_r$; the forward and reverse operating angular frequencies are ω_f and ω_r, respectively. The resonant frequency of the LC parallel network composed of L_1 and C_1 is ω_1, the resonant frequency of the parallel network composed of L_2 and C_2 is ω_2, the resonant frequency of the series LC network composed of L_3 and C_3 is ω_3, and the resonant frequency of the series LC network composed of L_4 and C_4 is ω_4. The relationships between each parameter in Figure 2 satisfy

$$\begin{cases} \omega_4 < \omega_2 = \omega_f < \omega_r = \omega_1 < \omega_3 \\ \omega_1 = \omega_r = 2\pi f_r = 1/\sqrt{L_1 C_1} \\ \omega_2 = \omega_f = 2\pi f_f = 1/\sqrt{L_2 C_2} \\ \omega_3 = 1/\sqrt{L_3 C_3} \\ \omega_4 = 1/\sqrt{L_4 C_4} \end{cases} \tag{1}$$

Due to $\omega_2 = \omega_f$, when power is transmitted in the forward direction, the impedance of the parallel network composed of L_2 and C_2 on the secondary side is infinite, equivalent to an open circuit. The secondary side is equivalent to a series compensation network. At the forward operating frequency, the series LC network composed of L_3 and C_3 is capacitive, while the LC parallel network composed of L_1 and C_1 is inductive. The forward power transfer topology structure can be equivalent to a CLC-S topology with a constant-voltage output characteristic.

When power is transmitted in the forward direction (the operating frequency is f_f), the equivalent capacitance of the series network (i.e., L_3, C_3) C_{peqwf} can be derived, as

$$C_{peqwf} = \frac{C_3}{1 - \omega_f{}^2 L_3 C_3} \tag{2}$$

The equivalent inductance of the parallel network (i.e., L_1, C_1) L_{eqwf} can be derived as

$$L_{peqwf} = \frac{L_1}{1 - \omega_f{}^2 L_1 C_1} \tag{3}$$

The primary compensation topology structure for power transfer can be equivalent to a CLC compensation topology composed of C_{peqwf}, L_{peqwf}, and C_p. The parallel network is equivalent to an open circuit. The series network (i.e., L_4, C_4) is equivalent to an inductor L_{seqwf}.

$$L_{seqwf} = L_4 - \frac{1}{\omega_f{}^2 C_4} \tag{4}$$

The equivalent circuit diagram of the forward power transfer channel is shown in Figure 3.

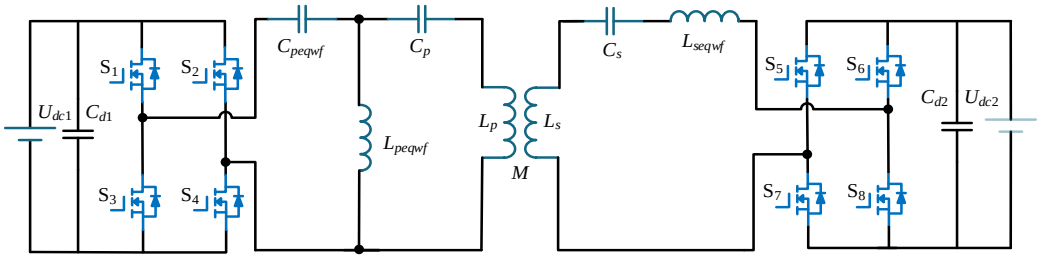

Figure 3. The equivalent circuit of the forward power transfer.

When power is transferred in the forward direction, the secondary side active bridge operates in rectification mode, and the inverter can be treated as a voltage source U_p and the load, while the rectifier is equivalent to a resistor *Rseq*. Based on First Harmonic Approximation (FHA), $U_p = \frac{2\sqrt{2}U_{dc1}}{\pi}$. The further equivalent circuit of the forward power transfer channel is shown in Figure 4.

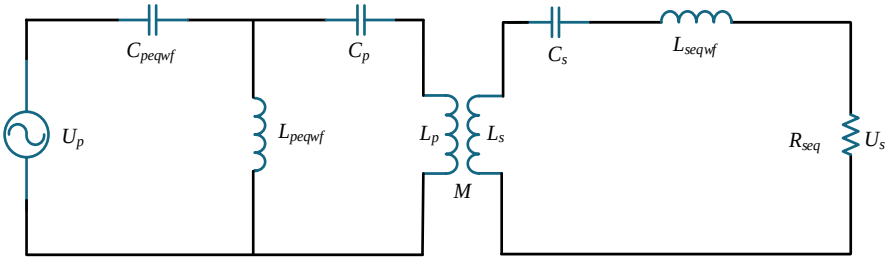

Figure 4. The further equivalent circuit of the forward power transfer.

The relationship between each parameter satisfies

$$\begin{cases} j\omega_f L_{peqwf} + \frac{1}{j\omega_f C_{peqwf}} = 0 \\ j\omega_f \left(L_p + L_{peqwf}\right) + \frac{1}{j\omega_f C_p} = 0 \\ j\omega_f \left(L_s + L_{seqwf}\right) + \frac{1}{j\omega_f C_s} = 0 \end{cases} \tag{5}$$

Based on (2), (3), and (5), The output current of the primary inverter can be derived as

$$\dot{I}_1 = \frac{2\sqrt{2}M^2(1-\omega_f{}^2 L_1 C_1)^2 U_{dc1}}{\pi R_{seq} L_1{}^2} \tag{6}$$

and the current of the primary coil can be obtained.

$$\dot{I}_p = \frac{2\sqrt{2}U_{dc1}(\omega_f{}^2 L_1 C_1 - 1)}{j\omega_f L_1 \pi} \tag{7}$$

The voltage transfer gain of the forward power transfer channel can be expressed as

$$G_f = \frac{U_{dc2}}{U_{dc1}} = \frac{M}{L_{peqwf}} = \frac{M(1-\omega_f{}^2 L_1 C_1)}{L_1} \tag{8}$$

When power is transmitted in reverse, due to $\omega_1 = \omega_r$, the parallel network composed of L_1 and C_1 on the primary side is equivalent to an open circuit, the series LC network composed of L_4 and C_4 on the secondary side is inductive, and the parallel network

composed of L_2 and C_2 is capacitive. The reverse power transfer topology structure can be equivalent to the LCC-S topology, and the system can achieve constant voltage output.

When power is transmitted in the reverse direction (the operating frequency is f_r), the equivalent inductance of the series network (i.e., L_4, C_4) L_{seqwr} can be derived,

$$L_{seqwr} = L_4 - \frac{1}{\omega_r{}^2 C_4} \tag{9}$$

The equivalent capacitance of the parallel network (i.e., L_2, C_2) C_{eqwr} can be derived as

$$C_{seqwr} = C_2 - \frac{1}{\omega_r{}^2 L_2} \tag{10}$$

The secondary compensation topology structure for reverse power transfer can be equivalent to an LCC compensation topology composed of L_{seqwr}, C_{seqwr}, and C_s. The parallel network is equivalent to an open circuit. The series network (i.e., L_3, C_3) is equivalent to a capacitor C_{peqwr}.

$$C_{peqwr} = \frac{C_3}{1 - \omega_r{}^2 L_3 C_3} \tag{11}$$

The equivalent circuit diagram of the reverse power transfer channel is shown in Figure 5.

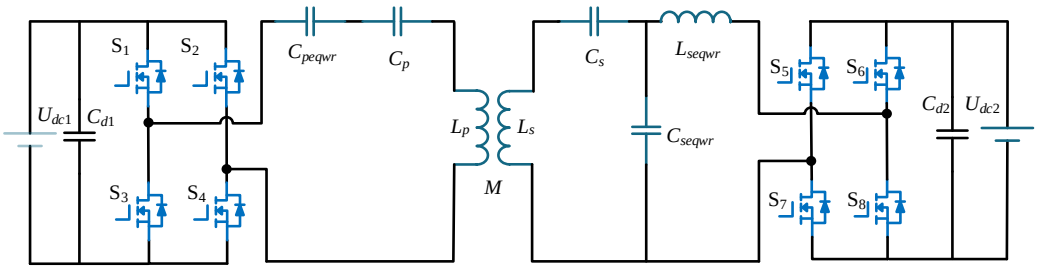

Figure 5. The equivalent circuit of the reverse power transfer.

The relationship between each parameter satisfies

$$\begin{cases} j\omega_r L_{seqwr} + \frac{1}{j\omega_r C_{seqwr}} = 0 \\ j\omega_r \left(L_s - L_{seqwr}\right) + \frac{1}{j\omega_r C_s} = 0 \\ j\omega_r L_p + \frac{1}{j\omega_r C_{peqwr}} + \frac{1}{j\omega_r C_p} = 0 \end{cases} \tag{12}$$

Similar to the forward power transfer, the voltage transfer gain of the reverse power transfer channel can be expressed as

$$G_r = \frac{U_{dc1}}{U_{dc2}} = \frac{M}{L_{seqwr}} = \frac{\omega_r{}^2 C_4 M}{\omega_r{}^2 L_4 C_4 - 1} \tag{13}$$

According to the voltage gain formula of the forward and reverse power transfer, when the input voltage of the system is constant, the magnitude of the output voltage is related to the value of the equivalent inductance (L_{peqwf} or L_{seqwr}) and M, and is independent of the load, which can enable it to achieve constant voltage output. In addition, the voltage transfer gain of both directions can be adjusted independently according to the applications. In order to replace the traditional contact slip ring equivalently, the voltage gain is set to 1 and the values of L_{peqwf} and L_{seqwr} are set to be equal to the value of M.

3.2. The Caliper Type Coupler

In some irregular rotating power supply scenarios, such as the traditional conductive slip ring structure shown in Figure 6a, this paper proposes a caliper-type coupler, as shown

in Figure 6b, that uses only a part of the nested outer cylinder structure to achieve power transfer. Compared with the traditional nested coupler shown in Figure 6c, the installation of the caliper-type coupler is more convenient, the system's flexibility is improved, and it is conducive to the replacement and maintenance of the slip ring.

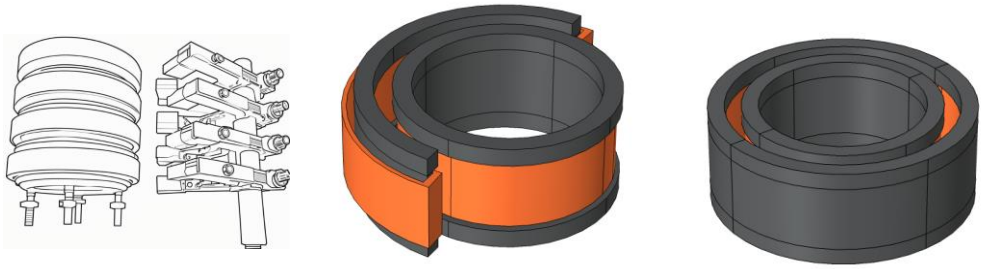

(a) (b) (c)

Figure 6. (**a**) The traditional conductive slip ring, (**b**) the proposed caliper type coupler and (**c**) the traditional nested coupler.

The dimension of the proposed caliper-type coupler is depicted in Figure 7. The inner and outer diameters of the coupler are 100 mm and 160 mm, respectively, the air gap between the inner and outer ring is 10 mm, and the height of the coupler is 60 mm. With the parameters listed in Table 1, the magnetic flux density map of the coupler obtained by applying a 5 A current excitation current to the primary and secondary sides of the coupler using magnetic field simulation software is shown in Figure 8.

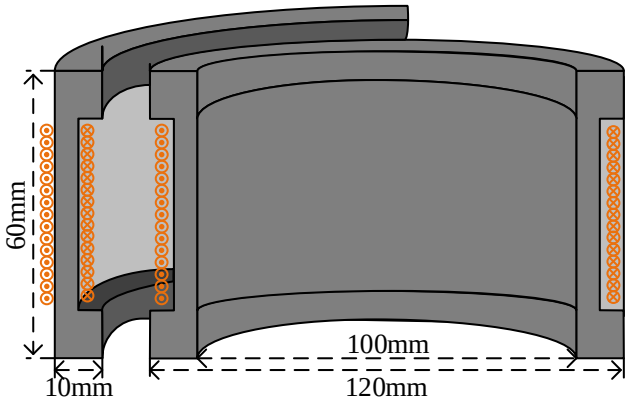

Figure 7. The dimensions of the proposed caliper-type coupler.

Table 1. The parameters of the coupler.

Symbols	Unit	Value
Air gap d	mm	10
Inner ring turns n_s	Turns	15
Outer ring turns	Turns	15
Outer ring curvature	Degree	90

When the excitation current increases, the magnetic flux density of the coupler increases. To avoid magnetic saturation, the analysis of the magnetic flux density in the x-axis direction of the system is shown in Figure 9. The maximum magnetic flux density of the system is 12 mT, which is lower than the magnetic saturation threshold of the magnetic core, and the system can work normally.

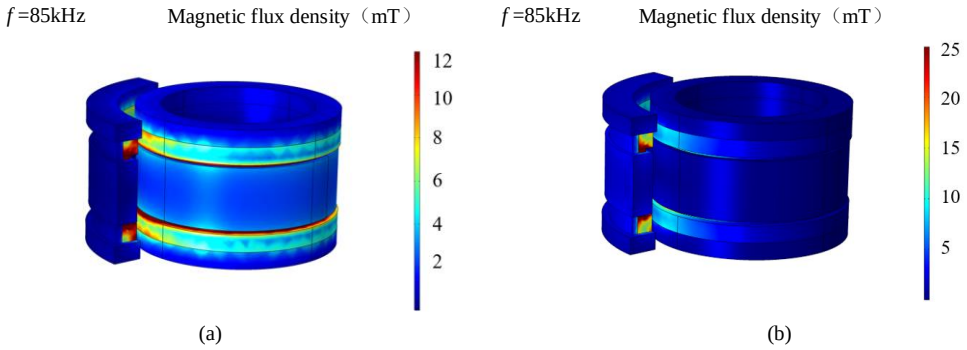

Figure 8. The magnetic flux density diagram of the coupler when the excitation current is applied to (**a**) the inner ring and (**b**) the outer ring.

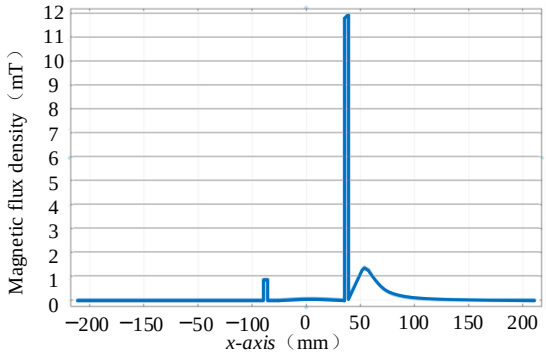

Figure 9. The magnetic flux density with the x coordinate.

4. Bidirectional Data Transfer Channel

Bidirectional data transfer is achieved through frequency division multiplexing coupling coils, using parallel connection to inject and extract the data carrier and adding an LC parallel network to achieve impedance isolation between the power carrier and data carrier [21]. The injection and extraction method of the BD-SWPDT data carrier is shown in Figure 10.

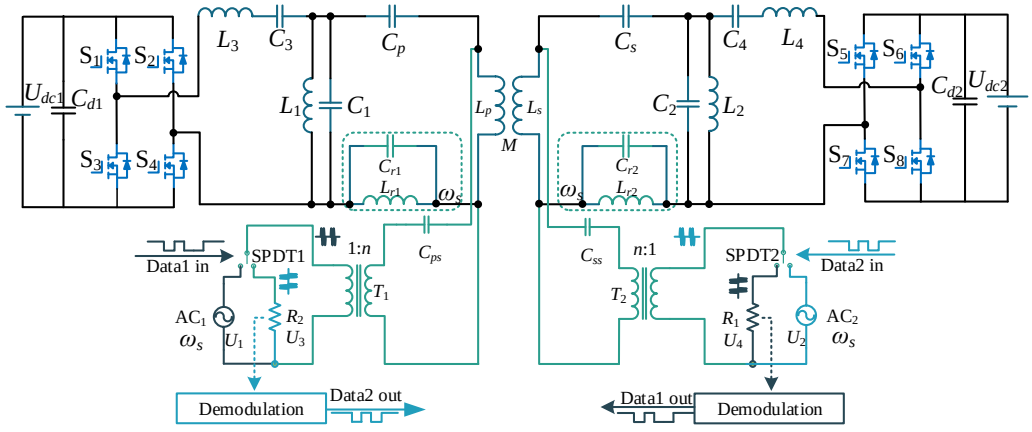

Figure 10. The data carrier injection and extraction.

The lower part of Figure 10 shows the data transfer channel. An LC parallel network is connected in series in the power transfer circuit, and the resonant frequency is set to the data carrier frequency f_s, which is much greater than that of the power carrier. When the data carrier is loaded to both ends of the coil, the impedance of the parallel network to the data carrier is relatively large, equivalent to an open circuit, and the equivalent circuit of the data transfer channel is shown in Figure 11. When the power transfer circuit is

working, the parallel network is equivalent to the inductor of the network at the power carrier frequency. The impact of the inductance on power transfer can be compensated for by connecting capacitors in series. Due to the pF level capacitance of C_{ps} and C_{ss}, the impedances of C_{ps} and C_{ss} are very large due to the relatively low-frequency power carrier, and the power carrier can barely flow through the data carrier processing circuit, thus achieving impedance isolation of the power and data transfer channels.

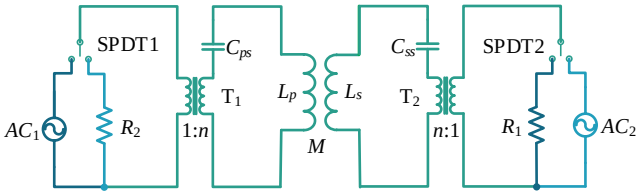

Figure 11. The equivalent circuit of the data transfer channel.

In the data transfer circuit, AC1 and AC2 are the data carrier voltage sources of the primary and secondary sides, respectively. The ASK modulation and loading of the data carrier are achieved by controlling the on–off of the analog switches SPDT1 and SPDT2. Transformers T1 and T2 are used to achieve electrical isolation between the data transfer circuit and the power transfer circuit. R_1 is the sampling resistor of the secondary side during forward data transfer, R_2 is the sampling resistor of the primary side during reverse data transfer, and the voltages of R_1 and R_2 are sampled for data demodulation. C_{ps} and C_{ss} are series compensation capacitors for the primary and secondary sides of the data transfer channel, and their values satisfy

$$\begin{cases} C_{ps} = \frac{1}{\omega_s{}^2 L_p} \\ C_{ss} = \frac{1}{\omega_s{}^2 L_s} \\ C_{r1} = \frac{1}{\omega_s{}^2 L_{r1}} \\ C_{r2} = \frac{1}{\omega_s{}^2 L_{r2}} \\ \omega_s = 2\pi f_s \end{cases} \tag{14}$$

It should be noted that f_s is much greater than f_f and f_r, the parallel networks (i.e., L_{r1}, C_{r1}, and L_{r2}, C_{r2}) can be treated as inductors Lr_1 and L_{r2}, respectively, at the relatively low-power transfer frequency, and the values of L_{r1}, and L_{r2} can be directly added to the values of L_p and L_s, respectively, when calculating the other parameters of the system.

Single-pole double throw switches SPDT1 and SPDT2 are connected to sampling resistors by default for receiving signals when there is no data transfer. When data are transmitted in the forward direction, the high- and low-level signals of the data control SPDT1 to modulate the high-frequency carrier. The modulated signal is transmitted to the primary side of transformer T1, and the voltage is stepped up by the transformer T1 and transmitted to the secondary side of transformer T2 through the SS compensation network. After the voltage is stepped down by transformer T2, a sine wave signal is received on resistor R_1, and then the data are demodulated through a data demodulation circuit. Due to the symmetrical structure design of the primary and secondary compensation network, the principle of data reverse transfer is consistent with that of forward transfer, thus enabling half duplex communication between the two sides of the wireless power system.

5. Experimental Verification

With the parameters listed in Table 2, an experimental prototype shown in Figure 12, built based on Figure 2 to verify the feasibility of the proposed BD-SWPDT system. The two auxiliary power supplies are used to power the data transceivers. Two USB to TTL converters are utilized to transmit and receive the data through the computer. A DC power supply (ITECH-IT6522C) is used as the DC power source and an electronic load

(ITECH-IT8813) is used as the load. In the data transceiver, a direct digital synthesizer (DDS, AD9833) is used to generate the high-frequency data carrier, an analog switch (ADG5419) is used to modulate the data carrier, and an operation amplifier (BUF634) is used as the high-speed buffer to drive the coils.

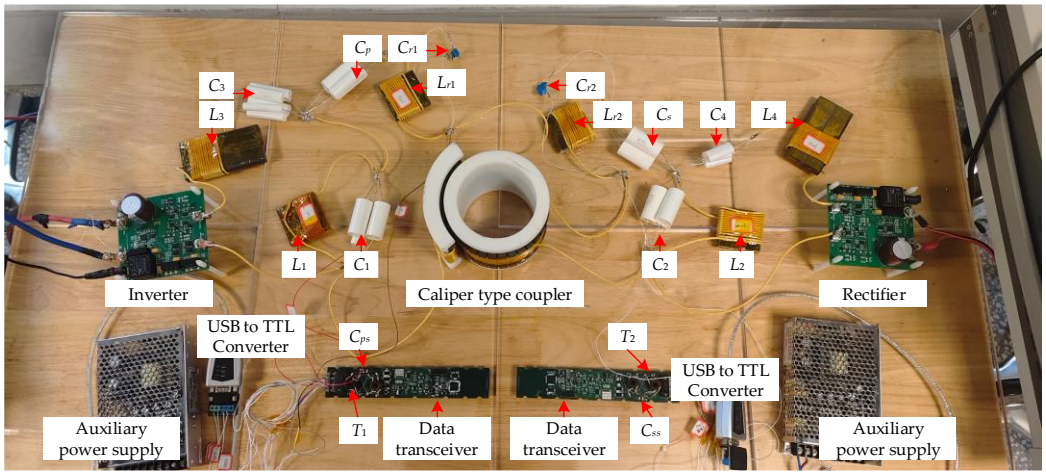

Figure 12. The experimental prototype.

Table 2. The parameters of the BD-SWPDT system.

Symbols	Unit	Values	Symbols	Unit	Values
U_{dc}	V	48	f_s	kHz	1500
f_f	kHz	85	f_r	kHz	105
L_p	μH	59	L_s	μH	109
M	μH	27.75	n	--	5
L_1	μH	9.5	L_2	μH	14.5
C_1	nF	241	C_2	nF	241
L_3	μH	30	L_4	μH	35
C_3	nF	61	C_4	nF	285
C_p	nF	34.5	C_s	nF	23.7
L_{r1}	μH	15	L_{r2}	μH	15
C_{r1}	pF	750	C_{r2}	pF	750
C_{ps}	pF	219	C_{ss}	pF	118

The procedures for the parameter design of the proposed system are depicted in detail in the flow chart shown in Figure 13. The values of L_{peqwf} and L_{seqwr} can be determined according to the mutual inductance and the transfer gain requirement of the practical application, and other parameters can be calculated from the equations listed.

When power is transferred in the forward and reverse directions, the waveforms of the power transfer channel under different output powers are shown in Figures 14 and 15, respectively. It can be seen from Figures 14 and 15 that the voltage of the inverter is slightly ahead of the inverter current, achieving zero voltage switch, the output voltage almost remains constant under different output powers, and the voltage transfer gain of the forward power transfer is the same with the reverse power transfer. The electronic load is set to constant power mode, and when the output power is 200 W, the efficiencies of the forward and reverse power transfer channel are 88.1% and 88.8%, respectively.

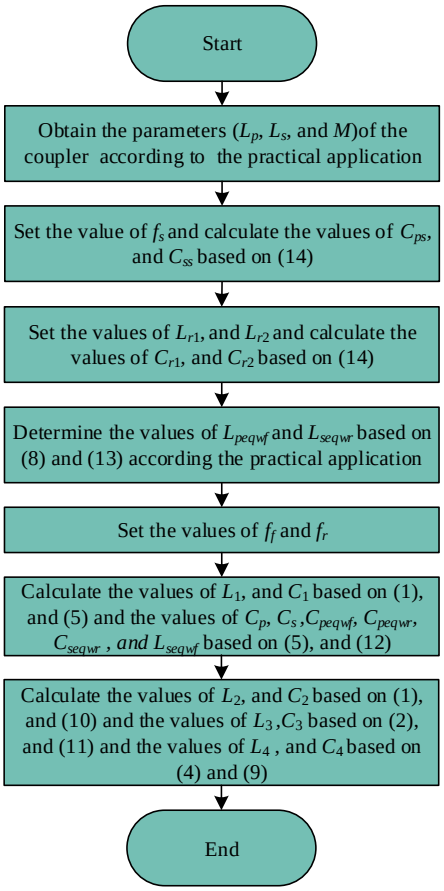

Figure 13. The flow chart used for parameter design.

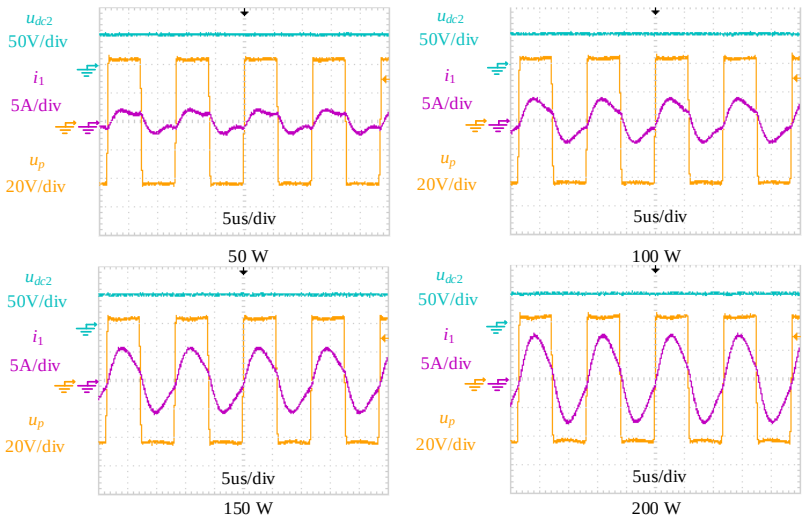

Figure 14. The waveforms of the forward power transfer channel under different output powers.

When there is only bidirectional data transfer (without simultaneous power transfer), the waveforms of the data transfer channel are shown in Figure 16. The transmitted data "Data1 in" are modulated and amplified to be converted into modulated signal U_1 (blue waveform), which is loaded onto both ends of the transformer. The secondary side receives the signal waveform U_4, as shown in the purple waveform, and after demodulation, the data "Data1 out" are restored, as shown in the green waveform. Since the waveforms of "Data1 in" and "Data1 out" are consistent, the data can be transmitted successfully.

As can also be seen from Figure 16, no interference occurs on the waveforms of the data transfer channel.

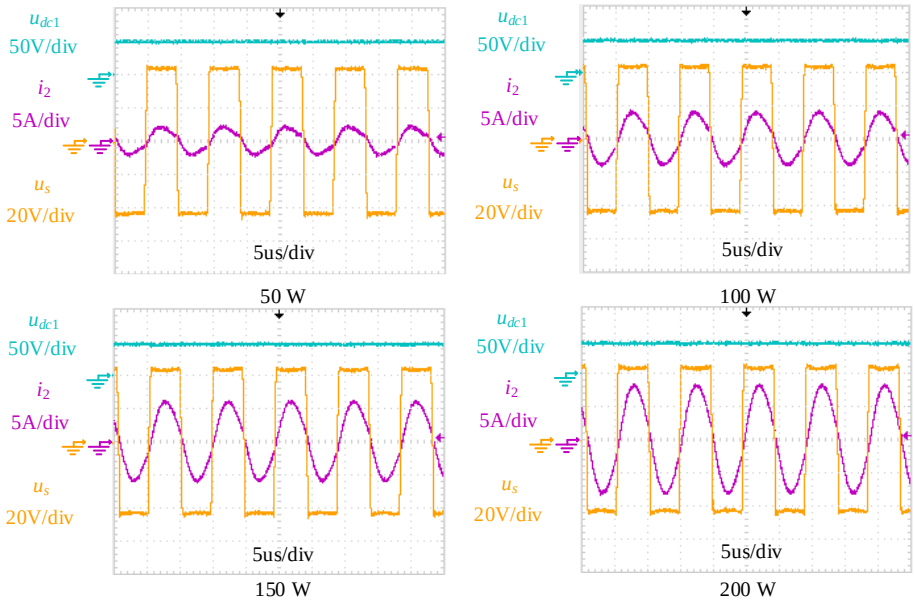

Figure 15. The waveforms of the reverse power transfer channel under different output powers.

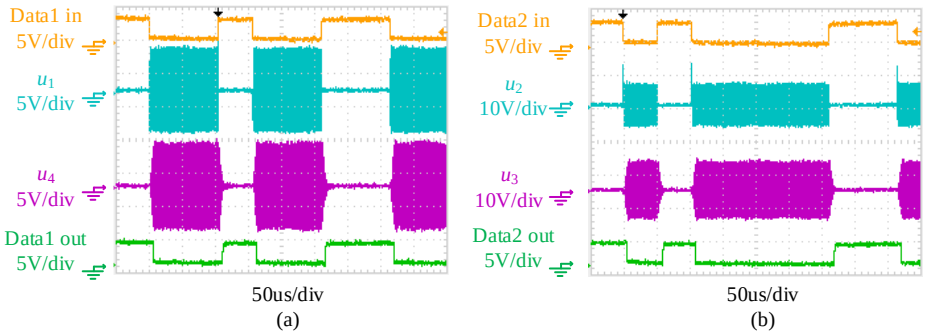

Figure 16. The waveforms of the data transfer channel, (**a**) forward data transfer and (**b**) reverse data transfer.

When power and data are transferred simultaneously, the power transfer channel will introduce interference to the data transfer channel, and the waveforms of the data transfer channel are shown in Figure 17. Comparing Figures 16 and 17, it can be inferred that the data transfer channel will be interfered with by the power transfer, but the interference is small, and almost does not affect the normal transfer of data.

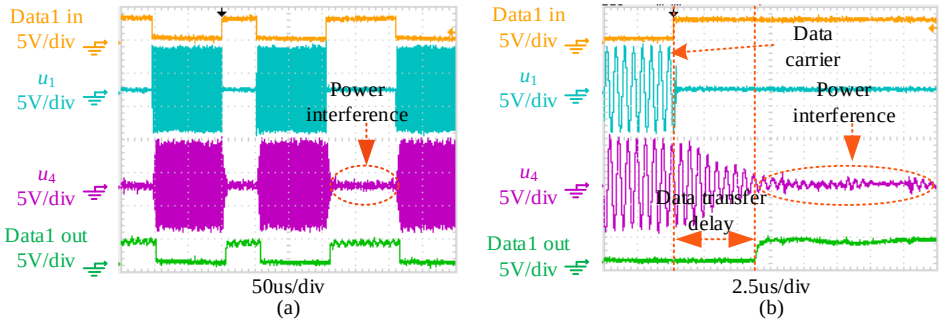

Figure 17. (**a**) The waveforms of the data transfer channel and (**b**) its stretched-out view with simultaneous power transferred.

The waveforms of the voltage of the coupled coils are also measured when power and data are transferred simultaneously, and are shown in Figure 18. It can be seen from the green circles that high-frequency waves are superimposed on the relatively low-frequency power carrier when the data carrier is transferred, which indicates that power and data are transferred simultaneously via the same coupled coils.

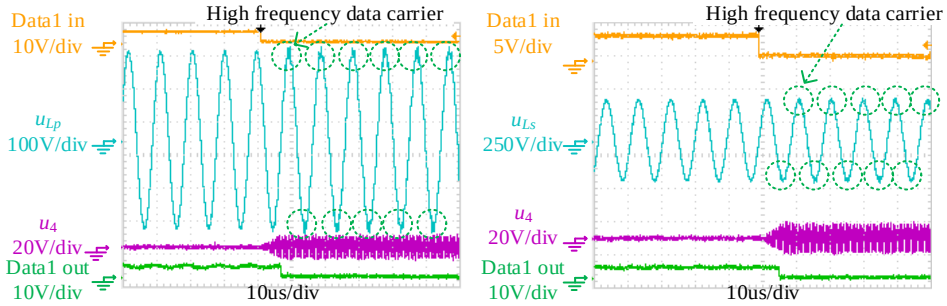

Figure 18. The waveforms of the data transfer channel and the voltage of the coupled coils.

To verify the effect of the proposed power transfer topology on the suppression of power interference, and due to the open circuit characteristics of the parallel networks (L_2, C_2) and (L_1, C_1) when power are transferred in the forward direction and the reverse direction, respectively, the waveforms of the data transfer channel are measured and shown in Figure 19. Here, power and data are transferred simultaneously with the LC parallel networks removed. Comparing Figure 19a,b, it can be inferred that the power interference can be significantly suppressed by the proposed topology, resulting in a high-quality transfer of data and reducing the complexity of the data demodulation circuit.

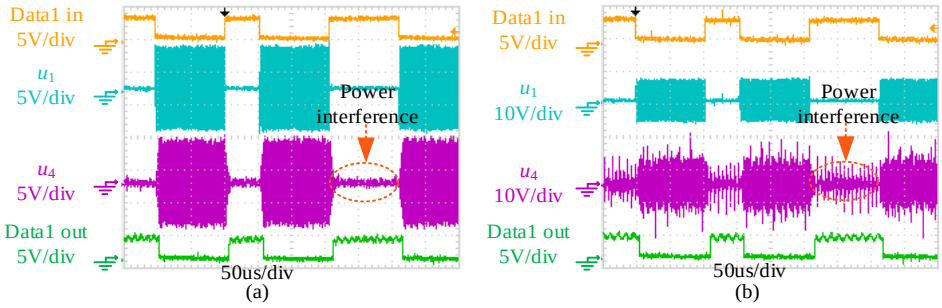

Figure 19. The waveforms of the data transfer channel (**a**) with the LC parallel network and (**b**) without the LC parallel network.

6. Results and Discussion

Table 3 summarizes the performance of this work and relevant works presented in [12,15,16,19–21]. It can be inferred from Table 3 that the coupler types of rotary applications can be roughly divided into four categories—the coaxial type, the planar type, the can type, and the caliper type. Due to the coupling structure, the maintenance of the coaxial nested coupler is more inconvenient than other types of couplers. The two sides of the coupler cannot be disassembled separately, which decreases the maintenance flexibility. In practical applications, besides the power transfer, data transfer is of equal importance. However, simultaneous data transfer is not applicable in [12,15,16], which limits its implementation in practical applications. SPWDT technology is proposed in [19–21], and this structure and two channels are formed to transfer power and data separately. However, in [20], extra coils are added to transfer data, which will increase the volume and complexity of the coupler. In this work, bidirectional power transfer is also achieved in addition to SWPDT sharing the power transfer coils, and the transfer gains of the two directions can be adjusted independently. When the power transfer channel operates, a large component of harmonics will be generated, which will cause EMI issues. In this work, compensation

networks with band-pass filtering characteristics are proposed, suppressing the EMI and creating a favorable condition for data transfer.

Table 3. The performance comparison among the technologies with rotary applications.

References	[12]	[15]	[16]	[19]	[20]	[21]	This Work
Data Transfer	N/A	N/A	N/A	Y	Y	Y	Y
Coupler Type	Coaxial Nested	Planar	Can type	Coaxial Nested	Coaxial Nested	Coaxial Nested	Caliper type
Maintenance Flexibility	Medium	High	High	Medium	Medium	Medium	High
Power Transfer Channels	Unidirectional 1	Unidirectional 1	Unidirectional 1	Unidirectional 2 (Shared)	Unidirectional 2 (Separate)	Unidirectional 2 (Shared)	Bidirectional 2 (Shared)
Harmonic Filtering	N/A	N/A	N/A	Y	N/A	N/A	Y

7. Conclusions

A non-contact slip ring system with bidirectional simultaneous wireless power and data transfer is proposed in this paper. A caliper-type rotary coupling structure is proposed. Compared with traditional coaxial nested slip rings, it has higher flexibility and easier disassembly and maintenance, and equivalent replacement can be achieved with traditional contact slip rings. The proposed bidirectional constant-voltage LC hybrid compensation topology not only achieves bidirectional constant voltage output, but also filters out most of the high-order harmonics in the power transfer channel, achieving simultaneous high-stability data transfer through the same coupler. The voltage transfer gain of both directions can be adjusted independently according to the application. Finally, the feasibility of the proposed BD-SWPDT system is verified by experiment.

Author Contributions: Methodology, Y.F., Q.C., S.W. and J.X.; validation, Q.C.; writing—original draft, Y.F. and S.W.; writing—review and editing, J.X.; supervision, Z.W. All authors have read and agreed to the published version of the manuscript.

Funding: This research received no external funding.

Data Availability Statement: The original contributions presented in the study are included in the article; further inquiries can be directed to the corresponding authors.

Conflicts of Interest: Author Jing Xiao was employed by the company Guangxi Power Grid Company Ltd., Nanning 530023, China. The remaining authors declare that the research was conducted in the absence of any commercial or financial relationships that could be construed as a potential conflict of interest.

References

1. Deng, P.; Tang, C.; Sun, M.; Liu, Z.; Hu, H.; Lin, T. EMI Suppression Method for LCC-S MC-WPT Systems by Parameter Optimization. *IEEE Trans. Power Electron.* **2024**, *39*, 11134–11147. [CrossRef]
2. Sun, Y.; Liao, Z.-J.; Ye, Z.-H.; Tang, C.-S.; Wang, P.-Y. Determining the Maximum Power Transfer Points for MC-WPT Systems with Arbitrary Number of Coils. *IEEE Trans. Power Electron.* **2018**, *33*, 9734–9743. [CrossRef]
3. Zhang, Z.; Georgiadis, A.; Cecati, C. Wireless Power Transfer for Smart Industrial and Home Applications. *IEEE Trans. Ind. Electron.* **2019**, *66*, 3959–3962. [CrossRef]
4. Lee, C.-H.; Ho, S.-T.; Hsu, S.-H.; Jiang, J.-A. Taguchi-Based Design of Planar Circular Coils Used in Wireless Charging of Mobile Phones. *IEEE Trans. Consum. Electron.* **2024**, *70*, 299–307. [CrossRef]
5. Deng, Z.; Hu, H.; Su, Y.; Chen, F.; Xiao, J.; Tang, C.; Lin, T. Design of a 60-kW EV Dynamic Wireless Power Transfer System with Dual Transmitters and Dual Receivers. *IEEE J. Emerg. Sel. Top. Power Electron.* **2024**, *12*, 316–327. [CrossRef]
6. Zhu, J.; Barmada, S.; Musolino, A.; Sani, L. Maintain Power Transmission and Efficiency Tracking Using Variable Capacitors for Dynamic WPT Systems. *Electronics* **2024**, *13*, 2853. [CrossRef]
7. Shah, I.A.; Zada, M.; Shah, S.A.A.; Basir, A.; Yoo, H. Flexible Metasurface-Coupled Efficient Wireless Power Transfer System for Implantable Devices. *IEEE Trans. Microw. Theory Tech.* **2024**, *72*, 2534–2547. [CrossRef]
8. Fernandez-Munoz, M.; Missous, M.; Sadeghi, M.; Lopez-Espi, P.L.; Sanchez-Montero, R.; Martinez-Rojas, J.A.; Diez-Jimenez, E. Fully Integrated Miniaturized Wireless Power Transfer Rectenna for Medical Applications Tested inside Biological Tissues. *Electronics* **2024**, *13*, 3159. [CrossRef]

9. Chen, C.; Jiang, C.; Wang, Y.; Fan, Y.; Luo, B.; Cheng, Y. Compact Curved Coupler With Novel Flexible Nanocrystalline Flake Ribbon Core for Autonomous Underwater Vehicles. *IEEE Trans. Power Electron.* **2024**, *39*, 53–57. [CrossRef]
10. Feng, Y.; Sun, Y.; Lin, T.; Hu, H.; Chen, F. Mutual inductance surrogate model of the UWPT system and its constant power optimization at misaligned positions. *Wirel. Power Transf.* **2024**, *11*, e001. [CrossRef]
11. Meng, W.; Hu, N.; Lan, H.; Lv, T. Lightweight Design of Magnetic Coupling Mechanism of Wireless Power Transfer System for Underground Rotary Guidance Device. In Proceedings of the 2024 10th International Conference on Power Electronics Systems and Applications (PESA), Hong Kong, China, 5–7 June 2024; pp. 1–4. [CrossRef]
12. Song, K.; Ma, B.; Yang, G.; Jiang, J.; Wei, R.; Zhang, H.; Zhu, C. A Rotation-Lightweight Wireless Power Transfer System for Solar Wing Driving. *IEEE Trans. Power Electron.* **2019**, *34*, 8816–8830. [CrossRef]
13. Zhou, Y.; Luo, Y.; Liu, S.; Li, D. An Efficient and Stable Embedded Multi-U-Shaped Column Rotary Transformer. *IEEE Trans. Power Electron.* **2023**, *38*, 6734–6743. [CrossRef]
14. Wang, L.; Li, J.; Luo, G.; Si, Q.; Guo, Z.; Peng, Y.; Robertson, I. A Mixed Flux Coupler and Dual-Path Parallel Compensation Based Rotating Wireless Power Transfer System Integrated with Rotational Speed Monitoring Function. *IEEE Trans. Power Electron.* **2024**, *39*, 7736–7751. [CrossRef]
15. He, X.; Shu, W.; Yu, B.; Ma, X. Wireless Power Transfer System for Rotary Parts Telemetry of Gas Turbine Engine. *Electronics* **2018**, *7*, 58. [CrossRef]
16. Trevisan, R.; Costanzo, A. A 1-kW contactless energy transfer system based on a rotary transformer for sealing rollers. *IEEE Trans. Ind. Electron.* **2014**, *61*, 6337–6345. [CrossRef]
17. Zhang, Y.; Yang, J.; Jiang, D.; Li, D.; Qu, R. Design, Manufacture, and Test of a Rotary Transformer for Contactless Power Transfer System. *IEEE Trans. Magn.* **2022**, *58*, 8400206. [CrossRef]
18. Li, T.; Wang, Y.; Lang, Z.; Qi, C.; Jin, X.; Chen, X.; Xu, D. Analysis and Design of Rotary Wireless Power Transfer System with Dual-Coupled XLC/S Compensation Topology. *IEEE Trans. Ind. Appl.* **2023**, *59*, 2639–2649. [CrossRef]
19. Fan, Y.; Hu, H.; Sun, Y.; Hu, H.; Wu, S. A Simultaneous Wireless Power and Coil Inductance Insensitive Data Transfer System for Rotary Structures. *IEEE Trans. Power Electron.* **2024**, *39*, 6526–6536. [CrossRef]
20. Li, X.; Li, Z.; Madawala, U.K.; Wang, H.; Sun, Y.; Dai, X.; Hu, J. A Simultaneous Wireless Power and Data Transfer Method Utilizing a Novel Coupler Design for Rotary Steerable Systems. *IEEE Trans. Power Electron.* **2024**, *39*, 11824–11833. [CrossRef]
21. Sun, Y.; Yan, P.-X.; Wang, Z.-H.; Luan, Y.-Y. The Parallel Transmission of Power and Data with the Shared Channel for an Inductive Power Transfer System. *IEEE Trans. Power Electron.* **2016**, *31*, 5495–5502. [CrossRef]